HAL
open science

# Holes and cracks in rigid foam films

Pauline C. Petit, Marie Le Merrer, Anne-Laure Biance

## To cite this version:

Pauline C. Petit, Marie Le Merrer, Anne-Laure Biance. Holes and cracks in rigid foam films. 2015. hal-01133820v1

## HAL Id: hal-01133820
## https://hal.science/hal-01133820v1

Preprint submitted on 20 Mar 2015 (v1), last revised 31 Mar 2015 (v2)

**HAL** is a multi-disciplinary open access archive for the deposit and dissemination of scientific research documents, whether they are published or not. The documents may come from teaching and research institutions in France or abroad, or from public or private research centers.

L'archive ouverte pluridisciplinaire **HAL**, est destinée au dépôt et à la diffusion de documents scientifiques de niveau recherche, publiés ou non, émanant des établissements d'enseignement et de recherche français ou étrangers, des laboratoires publics ou privés.

# Holes and cracks in rigid foam films

P. C. Petit, M. Le Merrer, A.-L. Biance
*Institut Lumière Matière, Université de Lyon, UMR5306 Université Lyon 1-CNRS, 69622 Villeurbanne, France*
(Dated: March 20, 2015)

The classical problem of foam film rupture dynamics has been investigated when surfaces exhibit very high rigidity due to the presence of specific surfactants. Two new features are reported. First a strong deviation to the well-known Taylor-Culick law is observed. Then, crack-like patterns can be visualized in the film; these patterns are shown to appear at a well defined deformation. The key role of surface active material on these features is quantitatively investigated, pointing the importance of surface elasticity to describe these fast dynamical processes, and thus providing an alternative tool to characterize surface elasticity in conditions extremely far from equilibrium. The origin of the cracks and their consequences on film rupturing dynamics are also discussed.

Despite its apparent useless character and simplicity, the dynamics of bursting of soap bubbles have fascinated scientists for more than a century. Lucien Bull (1904) made the first images of soap bubble bursts. The first theoretical analysis dates back to Dupré and then to Taylor [1] and Culick [2] where they considered the presence of a rim at the edge of a hole created in the liquid film, collecting the liquid during its movement. The constant hole opening velocity $V_c$ results from a balance between the rim inertia and surface tension in the film, and is given by $V_c = \sqrt{2\gamma_{\rm eq}/(\rho h_0)}$, with $\gamma_{\rm eq}$ the equilibrium surface tension, $\rho$ the liquid density and $h_0$ the film thickness. These results are in good agreement with stationary experiments performed on liquid sheet [1] and has been extensively investigated by McEntee and Mysels in the case of soap films [3] thicker than 50 nm. More recently, satellite formation during edge retraction [4] and bubble entrapment [5] have been investigated as these behaviors are crucial in many applications. Destabilization of liquid sheets or bubbles indeed arise in many practical situations ranging from the building material industry, when glass sheets are molded, to foam engineering, food processing, biological membrane and environmental science [5]. In these applications, liquids can be viscous or contain surface active materials. In the latter, surface tension becomes a dynamical quantity, which depends on the local surface concentration of surfactants, and thus on the elongation of the surface; this is characterized by the surface elasticity defined as the derivative of surface tension with respect to relative changes in surface area. The effect of surface elasticity has been observed through the development of an aureole surrounding the opening hole and expanding with time [6–8]. However, except in the case of very viscous liquid, the opening dynamics always obey Taylor-Culick law, although some deviations have been reported by Mysels [3, 9], but hardly commented. In this work, we investigate the dynamics of bursting of circular foam films generated from surfactant solutions inducing large surface elasticities and we report for the first time systematic deviations to Taylor-Culick law. A careful analysis allows us to estimate surface elasticity at both large compression and compression rate

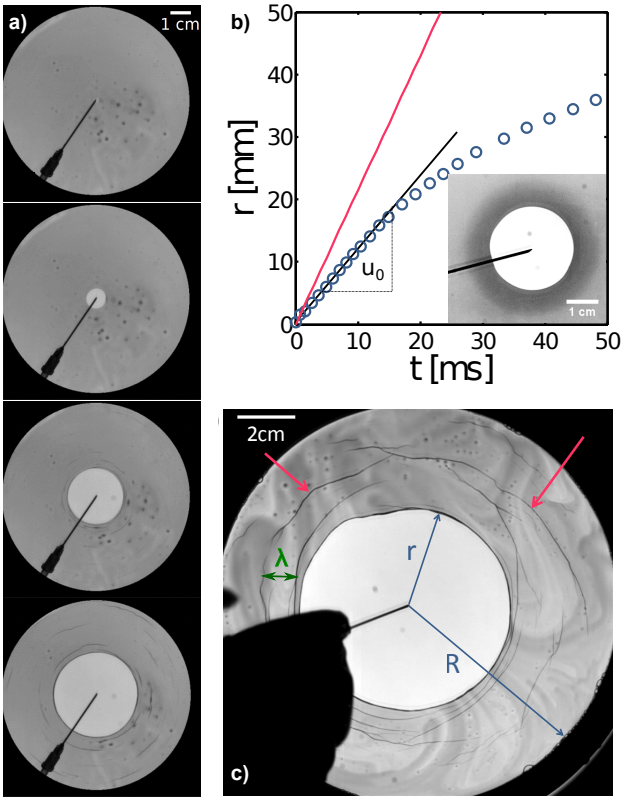


FIG. 1: (a) Image sequence of a foam film rupture ($h_0$=10 $\mu$m, solution E – Table I). The timelapse between images is 8 ms. (b) Radius $r$ of the hole *vs* time $t$ ($h_0$=10 $\mu$m, solution E). The red (light) line represents the prediction of Taylor-Culick, while the black line shows the initial opening at constant velocity $u_0$. Inset: Picture of a ruptured foam film (solution C) which highlights aureole formation. (c) Picture of a foam film (solution E) 37 ms after its breaking. The arrows highlight crack-like patterns, which appear during the hole opening.

in good agreement with reported data in the literature. Moreover, unexpected effects of frame size are observed through the appearance of new patterns, reminiscent of fractures or wrinkles in the film.

The experimental set-up consists in a circular metallic frame of radius $R = 1.5 - 11$ cm pulled out from a surfac-

| solution | A | B | C | D | E | F |
|---|---|---|---|---|---|---|
| $C$ [mM] | - | 0.055 | 0.11 | 0.22 | 0.88 | 2.2 |
| $\gamma_{eq}$ [mN/m] | 29 | 29 | 27 | 26 | 23 | 22 |
| $E_{od}$ [mN/m] | 4 | 50 | 90 | 200 | 400 | 400 |
| $E_0(u_0)$ [mN/m] | 60 | 200 | 2000 | 5000 | $2.10^4$ | $4.10^4$ |
| $E_0$(cracks) [mN/m] | - | - | 90 | 200 | 300 | 300 |

TABLE I: Properties of the surfactant solutions used in the experiments: MAc concentration $C$, equilibrium surface tension $\gamma_{eq}$ and surface elasticities. Data from Mitrinova *et al.* [12] for similar solutions (without glycerol and dye) are reported for $\gamma_{eq}$ and the elastic modulus $E_{od}$ measured with the oscillating drop method for small deformation ($0.2-4$ %) at frequency 0.2 Hz. $E_0(u_0)$ corresponds to the elasticity deduced from the initial hole velocity using Eq.1. $E_0$(cracks) corresponds to the elasticity deduced from cracking radius using Eq.2.

tant solution at different velocities to generate films with various thicknesses. The film absolute thickness is determined through an absorption technique measurement [10, 11] and we denote $h_0$ the initial average thickness of the film. Film rupture is initiated by approaching a heated needle and is recorded via a high-speed camera (10000 Hz, Photron SA-4). An image sequence is reported in Fig. 1(a), where we measure the radius $r$ of the expanding hole versus time, as shown in Fig. 1(b). Surfactant solutions are produced in a 10%-90% glycerol-water mixture in which a dye (Brilliant Black BN 60%, Sigma, 5g/L) is added. They contain 3.3 g.L$^{-1}$ of sodium lauryl-dioxyethylene sulfate (SLES, Stepan), 1.7 g.L$^{-1}$ of cocoamidopropyl betaine (CAPB, Goldschmidt) and myristic acid (MAc, Fluka) in the concentrations $C$ described in table I. The surface elasticities of similar solutions are well characterized in the literature [12] and span over two orders of magnitude when the concentration $C$ of MAc is varied as reported in table I. Such elastic moduli are attributed to the surface properties of the adsorbed layer of MAc, whose surface concentration is expected to increase with $C$ up to the saturation of the surface [13]. At the same time, micelles of the two co-surfactants (SLES and CAPB) help to solubilize the poorly soluble fatty acid.

Some remarkable features can be underlined. At first, the opening velocity is constant as expected but smaller than predicted by Taylor-Culick law (Fig. 1(b)). Moreover, an aureole already described in the past [6–8] is observed through spatial variations of transmitted light, especially for the less rigid interfaces (inset of Fig. 1(b) and S.I. [14]). Then, some dark patterns are observed (see arrows in Fig. 1(c)), which we denote *cracks* in the following. This apparition coincides with a decrease of the opening velocity (Fig. 1(b)), the presence of these cracks modifying the bursting dynamics.

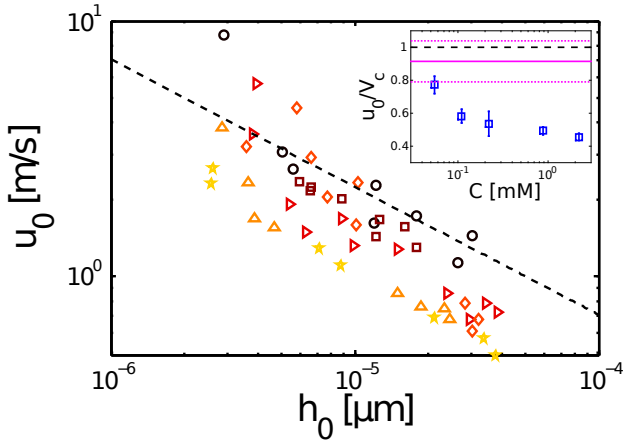


FIG. 2: Initial opening velocity $u_0$ of the hole as a function of the film thickness $h_0$ for $R = 3$ cm. The MAc concentration $C$ decreases from dark to light points: solutions A (o), B (□), C (▷), D (◇), E(△) and F (⋆). Inset: initial opening velocity normalized by Culick velocity $u_0/V_c$ as a function of $C$ (error bars: 95 % confidence intervals). The magenta solid line shows the value measured for $C = 0$, with error bars shown by the dotted lines. The values $u_0/V_c$ are extracted by performing least square percentage fit for each solution, with weights taking into account the 1 $\mu$m error on thickness measurements. In both figures, the black dashed lines represent Taylor-Culick law.

The initial opening velocity $u_0$ is represented in Fig. 2 as a function of the initial film thickness $h_0$ for various solutions. Without MAc (solution A of table I), the velocity follows Taylor-Culick law (○), which is consistent with interfaces of low elasticity. However, in the presence of MAc, the initial velocity is lower than in the previous case. For each MAc concentration, the initial velocity varies with $1/\sqrt{h_0} \propto V_c$. For each solution and different thicknesses, we thus extract the initial opening velocity normalized by Culick velocity. This quantity decreases when the MAc concentration increases (inset of Fig. 2), that is, for larger surface elastic moduli [12].

During the film opening, orthoradial cracks (perpendicular to the direction of opening) appear in the film (Fig. 1(a) and (c) and S.I. [14]), at a well defined radius of the hole $r_p$. Some specific irregular fold-like patterns and filaments have been previously reported by McEntee and Mysels [3], although not directly comparable to our observations. For a given solution, the inset of Fig. 3 shows that the ratio $r_p/R$ is independent of the frame radius (for $R = 1.5 - 11$ cm) and almost independent of the film thickness (for $h_0 = 2 - 20$ $\mu$m). The cracks thus appear for a well-defined critical compression of the interface. Fig. 3 shows that this critical compression decreases with MAc concentration and the surface modulus.

These two observations concerning the initial opening velocity and the onset compression for cracks can be rationalized following the framework initially proposed by Frankel and Mysels for the theoretical description of au-

reoles [15]. They considered that surfactants are insoluble, which is reasonable at the timescale considered here: the duration of the opening $R/u_0$, typically 30 ms, is smaller than surfactant desorption time $\tau$. Indeed, although these processes are likely to be dominated by surfactant exchange with micelles in our systems [13], a lower bound for $\tau$ is provided by the diffusion time across the film thickness $h_0^2/D \approx 40$ ms$-2$ s (for $h_0 = 2-40$ $\mu$m and $D = 10^{-10}$ m$^2$/s). Adsorption times longer than 30 ms for myristic acid in these systems have also been reported [16]. A compressive shock thus propagates at the surface of the film. The liquid is collected in an extended rim — an *aureole* — visible in Fig. 1(b) (inset) and whose shape depends on surface tension, film thickness and surface elasticity.

Viscous effects have also been neglected. Indeed, as no shear takes place within the film thickness, the characteristic Reynolds number and *surface* Reynolds numbers read $\mathrm{Re} = u_0 R/\nu \leq 1$ and $\mathrm{Re_s} = \rho u_0 R h_0/\kappa$, respectively, with $\nu$ the kinematic bulk viscosity and $\kappa$ the intrinsic surface viscosity. Surface viscous dissipation can *a priori* not be neglected if values of $\kappa$ measured at 0.2 Hz are considered [13, 17]. However, surface viscosity is expected to collapse at large frequencies, as shown in experiments and modeling [18]. Eventually, the observation of a constant initial velocity varying with $1/\sqrt{h_0} \propto V_c$ (Fig. 1(b) and 2) is a key indication that inertia (and not viscous effects) is dominant in this problem.

The dynamics of the rim is then controlled by the balance between inertia and surface tension spatial gradient. We assume here that surface elasticity is constant up to a certain compression. In this particular case, the velocity of the aureole front (delimiting the frontier with the zone of undisturbed film whose thickness is still $h = h_0$) simply reads $u_f = \sqrt{2E_0/(\rho h_0)} = V_C\sqrt{E_0/\gamma_{\mathrm{eq}}}$, which can be seen as a two dimensional analogous of sound (compression) velocity. The opening hole velocity can also be determined by solving the self-similar profile of the aureole and applying mass conservation. No analytical solution is provided in the considered radial geometry but numerical resolution shows that

$$u_0 = V_c\ f(E_0/\gamma_{\mathrm{eq}}) \tag{1}$$

with $f$ a decreasing function determined numerically (see SI [14]) and reported in Fig. 4. It is thus still proportional to Taylor-Culick velocity $V_c$ and decreases with the interfacial elasticity $E_0$, which is consistent with experimental observations of Fig. 2. From these data and Eq.1, an interfacial elasticity $E_0(u_0)$ can be deduced (Fig. 4), which is reported in Table I as a function of the MAc concentration. These data are compared to measurements of surface moduli $E_{\mathrm{od}}$ from the oscillating drop method performed by Mitrinova *et al* [12]. It shows the same qualitative variation with $C$ despite a discrepancy on the absolute values obtained. However, the shrinkage amplitude and the compression timescales differ by several orders of magnitude, and the surfactant monolayer at the interface is expected to be highly non-Newtonian [17, 18].

Besides, snapshot inspection shows that cracks appear when the compressive surface wave (i.e. the aureole front) reaches the metallic frame of the film. Cracks are thus expected for:

$$\frac{r_p}{R} = \frac{u_0}{u_f} = \sqrt{\frac{\gamma_{\mathrm{eq}}}{E_0}}\, f\left(\frac{E_0}{\gamma_{\mathrm{eq}}}\right) \tag{2}$$

This prediction, represented in Fig. 4, is indeed in good agreement with our observations: The hole radius when

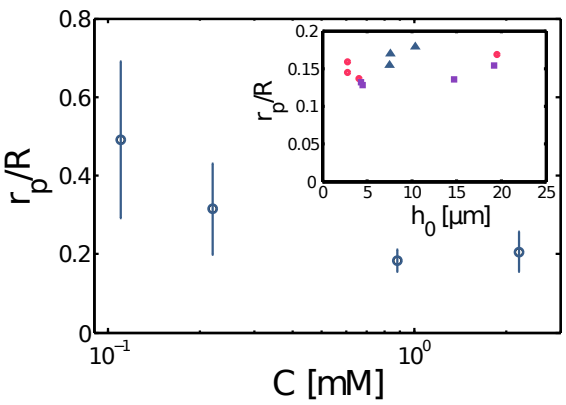


FIG. 3: Critical compression of the interface for crack formation $r_P/R$ averaged for thicknesses $h_0 = 2-35$ $\mu$m and $R = 3$ cm, as a function of MAc concentration $C$. Inset: $r_P/R$ as a function of the initial thickness $h_0$ for solution E and different frame radii $R = 1.5$ cm (o), $R = 3$ cm (□) et $R = 11$ cm (△).

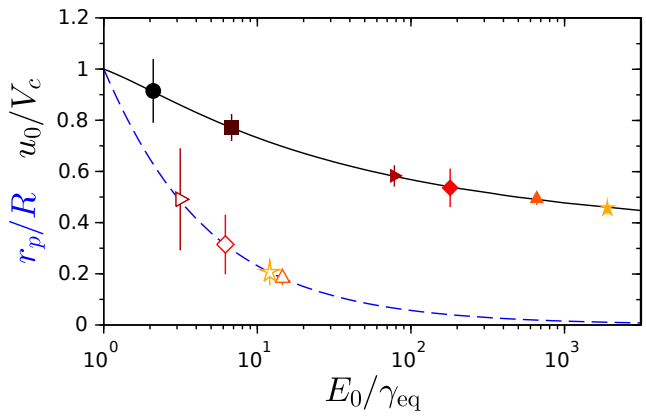


FIG. 4: Solid black line: theoretical prediction for the normalized hole velocity $u_0/V_c = f(E_0/\gamma_{\mathrm{eq}})$ for radial bursting (Eq.1 and S.I. [14]). Blue dashed line: prediction for the critical radius at which cracks appear $r_P/R = \sqrt{\gamma_{\mathrm{eq}}/E_0} f(E_0/\gamma_{eq})$ (Eq.2). The solid (resp. empty) symbols correspond to the experimental data from Fig. 2 (resp. Fig. 3), from which we determine the elastic moduli $E_0(u_0)$ (resp. $E_0$(cracks)). Same symbols and colors as in Fig. 2.

cracks appear $r_p$ increases with the frame radius $R$ and decreases with surface elasticity probed through MAc concentration variations, as shown in Fig. 3. Eventually, this critical compression does not depend on film thickness $h_0$, showing that elasticity is not affected by confinement in the experimental configuration tested.

The surface elasticity $E_0$(cracks) can therefore be deduced from the critical radius for crack apparition $r_p$ (Fig. 4), and reported for the different MAc concentration in table I. In this case, a very good agreement is obtained with the measured value of the surface modulus [12], which confirms that the cracks arise from a compression of the aureole when its front reaches the frame.

Note that the values of surface elasticity deduced from our two methods may differ. This is however expected due to our strong hypothesis of constant elasticity. Indeed, while the aureole front velocity only depends on the surface elasticity at very low compression rate (at the edge of the undisturbed film), the hole opening velocity modeling takes into account the elasticity through large interface compression. For large deformation, it is expected that the constant elasticity model fails: at large compression, the myristic acid surface concentration increases, which should result in larger elasticity as can be inferred from the moduli dependency upon $C$ [12]. The effective modulus $E_0(u_0)$ should then deviate more from measurements at small deformations performed by the oscillating bubble technique [12].

In addition, the effect of elasticity has indirect consequences of some features of foam film rupture. For example, no flapping nor transverse destabilization of the rim was observed for our rigid soap films, in contrast to observations on low elasticity films and theoretical predictions [4]; however, the reduced rim velocity could prevent the flapping instability to develop and subsequent film atomization [4].

Let us now discuss the observed crack-like patterns. During the fast deformation of the surface, the surfactants behave as an insoluble monolayer, comparable to a lipid monolayer experiencing a compression in a Langmuir trough [19]. In this case, above a critical compression, such a monolayer can behave differently depending on its structure. If it is liquid-like, it ejects the molecules in the bulk in the form of vesicles or bilayers. If it is solid-like, it can bend as an elastic sheet or fracture as a fragile material.

Although our experiment does not provide a microscopic characterization of this transient surface structure, the crack pattern can be macroscopically characterized. In particular, even though the cracks are irregularly distributed, a number of cracks per radial segment can be counted; the deduced characteristic length between two cracks denoted $\lambda$ (Fig. 1(c)) is reported in Fig. 5 as a function of MAc concentration $C$ (a) and film thickness $h_0$ (b).

The increase of $\lambda$ with $C$ is expected whatever the

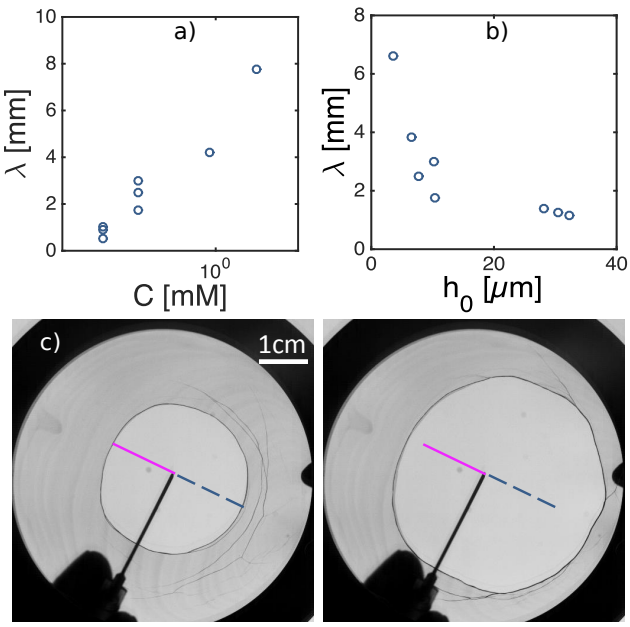


FIG. 5: (a) Characteristic length $\lambda$ between two cracks as a function of MAc concentration $C$ for $h_0 = 11 \pm 3$ $\mu$m. (b) $\lambda$ as a function of the film thickness $h_0$ for solution D. (c) Bursting of a soap film of thickness $h_0 = 3$ $\mu$m (solution E). The timelapse between the two images is 9 ms, and the two lines highlight the velocity inhomogeneities. See videos in S.I. [14].

mechanism proposed. On the one hand, for higher bulk concentration, solubilization of interfacial surfactants is more difficult, hence a reduced number of vesicles or bilayers are to be expelled. On the other hand, a more concentrated solid-like layer will also exhibit a higher bending modulus and wavelength of elastic ripples are expected to increase with this modulus [20]. The decrease of the characteristic length with the film thickness $h_0$ is more unexpected. For the solid-like behavior, a thinner elastic sheet will bend more easily than a thicker one, thus exhibiting smaller ripple wavelength when buckled [21], in contrast with our observations. If cracks correspond to monolayer collapse by vesicles formation, it should not be affected by the film thickness. However, when modifying the thickness of the film, we also vary the velocity of compression or shrinkage rate. This parameter induces dynamical structural change in the surfactant monolayers (as it does in bulk crystallization processes for example [22]).

Finally, a complete understanding of the origin of these crack-like patterns would require some local high speed imaging structural analysis , which are beyond the scope of the present paper.

The presence of these irregular cracks have direct consequences on hole opening dynamics. Indeed, when the aureole reaches the metallic frame, the hole opening slows down (and even stops for the thinner rigid films) and then

irregularly accelerates in the region where the cracks appears. This feature is reported in Fig. 5(c). Moreover, a velocity discontinuity in the liquid is observed, the outer region being at rest whereas the inner region is deformed.

To conclude, we have shown that modifying the chemistry of surfactant solutions can have strong influences on macroscopic dynamical processes, as observed in various situations in foams and foam films [11, 23–26]. However, we have investigated here this effect under large deformations and in a fast dynamical process, *i.e.* at large Reynolds numbers, where the effects of molecular scales and surfactants are expected to be negligible.

The initial constant velocity opening dynamics is well described taking into account the surface elasticity of the interfaces and was shown to be reduced at high surface modulus. This may be responsible for the inhibition of rim fragmentation and droplet ejection usually reported in liquid film ruptures [4]. Further studies should determine the role of the ejected droplets in rupture propagation in macroscopic foams; the stability of these systems is indeed known to depend dramatically on the surface elastic properties [27]. However, finite size effects becomes soon crucial: when the elastic compression surface wave reaches the border of the frame, crack-like patterns, where velocity discontinuity are observed, appear in the foam film. Determining the origin of cracks, their microscopic structure, their location and number, and how they control film opening dynamics remain a challenge to tackle.

The authors thank Gilles Simon for his help in setting up the experiment.


[1] G. Taylor, Proceedings of the Royal Society of London Series A-mathematical and Physical Sciences **253**, 313 (1959).

[2] F. E. C. Culick, Journal of Applied Physics **31**, 1128 (1960).

[3] W. R. McEntee and K. J. Mysels, Journal of Physical Chemistry **73**, 3018 (1969).

[4] H. Lhuissier and E. Villermaux, Physical Review Letters **103**, 054501 (2009).

[5] J. C. Bird, R. de Ruiter, L. Courbin, and H. A. Stone, Nature **465**, 759 (2010).

[6] A. T. Florence and G. Frens, Journal of Physical Chemistry **76**, 3024 (1972).

[7] N. Y. Liang, C. K. Chan, and H. J. Choi, Physical Review E **54**, R3117 (1996).

[8] H. Lhuissier and E. Villermaux, Comptes Rendus Mecanique **337**, 469 (2009).

[9] A. T. Florence and K. J. Mysels, The Journal of Physical Chemistry **78**, 234 (1974).

[10] H. Lastakowski, F. Boyer, A. L. Biance, C. Pirat, and C. Ybert, Journal of Fluid Mechanics **747**, 103 (2014).

[11] P. Petit, J. Seiwert, I. Cantat, and A.-L. Biance, Journal of Fluid Mechanics **763**, 286 (2015).

[12] Z. Mitrinova, S. Tcholakova, K. Golemanov, N. Denkov, M. Vethamuthu, and K. P. Ananthapadmanabhan, Colloids and Surfaces A-physicochemical and Engineering Aspects **438**, 186 (2013).

[13] K. Golemanov, N. D. Denkov, S. Tcholakova, M. Vethamuthu, and A. Lips, Langmuir **24**, 9956 (2008).

[14] *Supplementary information available at:*.

[15] S. Frankel and K. J. Mysels, Journal of Physical Chemistry **73**, 3028 (1969).

[16] Z. Mitrinova, S. Tcholakova, Z. Popova, N. Denkov, B. R. Dasgupta, and K. P. Ananthapadmanabhan, Langmuir **29**, 8255 (2013).

[17] S. Costa, Ph.D. thesis, Université Paris-Est Marne La Vallée (2012).

[18] J. Lucassen and M. V. D. Tempel, Chemical Engineering Science **27**, 1283 (1972).

[19] K. Y. C. Lee, Annu. Rev. Phys. Chem. **59**, 771 (2008).

[20] E. Cerda and L. Mahadevan, Physical Review Letters **90**, 074302 (2003).

[21] L. D. Landau and E. M. Lifshitz, *Elasticity Theory* (Pergamon Press, Oxford, 1975).

[22] B. Cabane and S. Hénon, *Liquides– Solutions, dispersions, gels* (Belin, 2003).

[23] Y. Couder, J. M. Chomaz, and M. Rabaud, Phys. D **37**, 384 (1989).

[24] M. Durand and H. A. Stone, Physical Review Letters **97**, 226101 (2006).

[25] J. Seiwert, M. Monloubou, B. Dollet, and I. Cantat, Physical Review Letters **111**, 094501 (2013).

[26] E. Lorenceau, N. Louvet, F. Rouyer, and O. Pitois, Eur. Phys. J. E **28**, 293 (2009).

[27] E. Rio and A.-L. Biance, ChemPhysChem **15**, 3692 (2014).